RSC Advances

PAPER

View Article Online
View Journal | View Issue

Cite this: *RSC Adv.*, 2021, **11**, 21560

Choline chloride-based deep eutectic solvents as effective electrolytes for dye-sensitized solar cells†

De Nguyen,[ac] Tuan Van Huynh,[bc] Vinh Son Nguyen,[d] Phuong-Lien Doan Cao,[ce] Hai Truong Nguyen,[ce] Tzu-Chien Wei,[d] Phuong Hoang Tran *[ce] and Phuong Tuyet Nguyen *[ac]

Electrolytes for dye-sensitized solar cells remain a challenge for large-scale production and commercialization, hindering the wide application of solar cells. We have developed two new electrolyte-based deep eutectic solvents using a mixture of choline chloride with urea and with ethylene glycol for dye-sensitized solar cells. The prominent features of the two deep eutectic solvent electrolytes are simple preparation for large-scale production with inexpensive, available, and nontoxic starting materials and biodegradability. The solar cell devices proceeded in a safe manner as the two deep eutectic solvents afforded low-cost technology and comparative conversion efficiency to a popular ionic liquid, namely 1-ethyl-3-methylimidazolium tetracyanoborate. Results showed that devices with choline chloride and urea electrolyte exhibited improved open circuit voltage values (V_{OC}), while the ones with choline chloride and ethylene glycol showed an increase in the short circuit current (I_{sc}). Characterization of the devices by electrochemical impedance spectroscopy helped explain the effects of their molecular structures on the enhancement of either V_{OC} or I_{sc} values. These new solvents expand the electrolyte choices for designing dye-sensitized solar cells, especially for the purpose of using low-cost and eco-friendly materials for massive production.

Received 27th April 2021
Accepted 31st May 2021

DOI: 10.1039/d1ra03273a

rsc.li/rsc-advances

1. Introduction

Dye-sensitized solar cells (DSCs) have attracted numerous scientific and technological interests as efficient and low-cost alternative photovoltaic devices compared to conventional solar cells.[1,2] Three important components of DSC include a TiO_2 loaded dye sensitizer photo-anode, a platinum cathode, and an electrolyte between the two electrodes.[2] A typical DSC electrolyte comprises a coupled redox mediator (*e.g.* I^-/I_3^-) and electrolyte additives dissolved in liquid or ionic liquid solvents. The first DSCs used liquid electrolytes and achieved high energy conversion efficiencies.[2,3] However, the required volatile and hazardous solvents often lead to leakage, which impedes the durability and photovoltaic performance of DSCs and damages the environment.[3–6] Such so-called "non-robust" electrolytes also caused a fast thermal degradation of ruthenium dyes,[7,8] key components in DSCs, leading to a loss in long-term photovoltaic performance of the devices.[8,9] Ionic liquid electrolytes have been thus developed as alternative electrolyte solvents[10,11] due to their non-volatility, high conductivity, and thermal stability.[12–14] However, the performance of DSCs with ionic liquid electrolyte still faces challenges including (i) high viscosity leading to low ionic diffusion of the mediator and hence low conversion efficiency of the devices;[15] (ii) high cost and low purity;[10] (iii) and potentially harmful effects from the electrolyte waste to the environment and human health.[11,16] Some alternative, low-viscosity ionic liquid electrolytes such as 1-ethyl-3-methylimidazolium dicyanamide,[17] imidazolium selenocyanate,[18] triethylammonium perfluorocarboxylate,[19] and imidazolium tetracyanoborate or imidazolium tricyanomethanide[20] have been subsequently studied as promising solvents for high-performance DSCs, but the economic and environmental issues remain. In the search for a more eco-friendly, low-cost, and efficient electrolyte for DSC devices, deep eutectic solvents (DESs) have been considered as potential candidates due to many of their advantages such as high availability and sustainability, simple and inexpensive manufacturing, and biodegradability.[21]

Deep eutectic solvents (DESs) were first described by Abbott and coworkers by mixing the substituted ammonium salts with

[a]Faculty of Chemistry, University of Science, Ho Chi Minh City, Vietnam. E-mail: ntphuong@hcmus.edu.vn
[b]Faculty of Physics and Engineering Physics, University of Science, Ho Chi Minh City, Vietnam
[c]Vietnam National University Ho Chi Minh City, Vietnam. E-mail: thphuong@hcmus.edu.vn
[d]Department of Chemical Engineering, National Tsing-Hua University, Hsinchu 30013, Taiwan
[e]Department of Organic Chemistry, Faculty of Chemistry, University of Science, Ho Chi Minh City, Vietnam

† Electronic supplementary information (ESI) available. See DOI: 10.1039/d1ra03273a

hydrogen bond donor components.[22–24] Up until now, several kinds of DESs have been fabricated by mixing two or three cheap and non-hazardous materials, which through hydrogen bonding interactions, have freezing points lower than the starting components.[25] As a result, DESs show better properties illustrating significant advantages for industrial application.[26] DESs can be prepared by simply mixing two or three components,[27] which are relatively inexpensive and environmentally friendly.[28,29] For example, choline chloride, also well-known as vitamin B_4 and as an additive in fish feed, is a useful quaternary ammonium salt to prepare DESs.[30] In a recent development, DESs have been used in a wide variety of applications, such as biotransformation,[31–33] catalysis,[34–36] extraction processes,[37–39] and material sciences.[40]

DESs are emerging as potential substitutes for ionic liquids in DSC electrolytes. Jhong *et al.* reported a eutectic mixture of glycerol and choline iodide as an electrolyte in DSCs with organic dye (D149) and achieved an efficiency of 3.88%.[41] Later on, Boldrini and coworkers applied an aqueous choline chloride-based DES as an electrolyte and phenothiazine organic sensitizer in DSC, which reached an efficiency of nearly 2%.[42] In 2019, our group mixed a choline chloride: phenol DES with the liquid electrolyte of acetonitrile as a solvent.[43] Results showed that even though the DES-added cells were initially less efficient than the DES-free ones, the efficiencies of the two devices became comparable after more than 1000 hours of operation. DES helped stabilize and improve the long-term photovoltaic performance of the DSC devices, particularly the short circuit current. However, further studies are needed to develop more eco-friendly, volatile organic solvent-free electrolytes.

To solve the problem, in this study, we developed two choline chloride-based DES mixtures with urea (DES-CU) and with ethylene glycol (DES-CE), for applications in DSC electrolytes. The electrolytes were prepared with redox mediator I^-/I_3^- and electrolyte additives in the DES without any addition of liquid solvents. The DES cells were characterized and analyzed by the current–voltage (*J–V*) curve; incident photon to current efficiency (IPCE), and electrochemical impedance spectroscopy (EIS) measurements in comparison with standard cells used the popular ionic liquid – 1-ethyl-3-methylimidazolium tetracyanoborate (EMITCB). The results demonstrated that the DES devices achieved comparative energy conversion efficiency to the standard ionic liquid devices. EIS analysis gave a finding of the DES molecular structures affecting the photovoltaic performance of the devices, especially on the open-circuit voltage (V_{OC}) and short circuit current density (J_{SC}) values.

2. Experimental

A. Preparation of DESs

DESs were prepared according to a previously reported procedure.[44] Specifically, DES-CE (choline chloride/ethylene glycol molar ratio of 1/2) and DES-CU (choline chloride/urea molar ratio of 1/2) were prepared by heating the corresponding individual pure components to 80 °C under stirring until a colorless solution was formed.

B. DSC fabrication & characterization

DSC fabrication. Fluorine-doped tin oxide (FTO) glass (Pilkington, USA; 8 Ω cm^{-2}) was cleaned with a detergent solution with ultrasonication, rinsed with deionized water and ethanol, then treated with 40 mM $TiCl_4$ (Sigma Aldrich) solution at 70 °C in 30 minutes before use. FTO glasses (1.5 × 1.5 cm) were subsequently screen printed with two different types of TiO_2 paste, mesoporous (Dyesol 18NR-T) and scattering (Solaronix R/SP), to form a 0.16 cm^2 square pattern with a total thickness of 12 μm. The thin films were annealed at 500 °C for 30 minutes. After cooling to room temperature, TiO_2 films were immersed in 0.3 mM N719 dye (Dyesol) solution in ethanol for 12 h. TiO_2 loaded dye photo-anodes were analyzed using UV-Vis absorption measurement to ensure that the dye loading reached maximum concentration and all TiO_2|N719 anodes were identical. The absorption spectra of the TiO_2|N719 anodes are shown in Fig. S1.†

The cathode was prepared by drilling two small holes in the 1.5 × 1.5 cm FTO glass, followed by cleaning and platinum paste (Dyesol PT1) deposition process.[45]

The reference EMITCB ionic liquid electrolyte comprises 1 M 1-methyl-3-propylimidazolium iodide (PMII), 0.2 M iodine (I_2), 0.1 M guanidinium thiocyanate (GuSCN), 0.5 M *N*-methylbenzimidazole (NMB), 0.74 M EMITCB, all from Sigma Aldrich. The DES-based electrolytes were prepared by replacing EMITCB with DES-CE or DES-CU. To optimize the electrolyte composition, different DES/EMITCB volume ratio, including 0.5 (CE0.5, CU0.5), 1 (CE1, CU1), 1.5 (CE1.5, CU1.5), were evaluated.

The electrolyte was then injected through the hole on the platinized cathode. Finally, another thin cover glass slide with the Surlyn film was hot-pressed to enclose the two holes. The complete DSC devices were kept in the dark for further characterization.

DSC characterization

J–V curve and IPCE measurement. A black mask with an active area of 0.16 cm^2 was attached to the photoanode. The *J–V* curve of DSC was measured with a computer-controlled digital source meter (Keithley 2400) under the exposure of a standard solar simulator (PECCELL, PEC-L15. AM1.5, Class B) with a light intensity of 1000 W m^{-2}, relative humidity around 30–40% at 20 °C.

IPCE was measured using a PEC-S20 (Peccell Technologies). The light wavelength was set from 300 to 900 nm with an increment of 5 nm.

EIS full cell in the dark. A Schlumberger SI 1255 HF frequency response analyzer integrated with an electrochemical interface SI 1286 was used to measure the EIS of fully assembled DSC cells in dark conditions with a frequency range of 10^5 Hz to 10^{-1}. The negative potentials of −0.4, −0.5, −0.6, −0.7 V were applied to the TiO_2 photo-anode during measurements. The obtained impedance spectra were fitted using the Z-view software to extract impedance parameters.

3. Results and discussion

A. Characterization of DES-CU and DES-CE

For pure choline chloride, vibrational bands at 3476 cm^{-1} refer to the presence of hydroxyls, while the bands at 3019–2965 cm^{-1}

and 1478–1376 cm^{-1} indicate the presence of an alkyl group (Fig. S2†). The characteristic C–N vibration can be found at 1135 cm^{-1}. The vibration bands at 1087 and 955 cm^{-1} are assigned to C–O and C–C–O asymmetric stretching associated with the $–CH_2CH_2–OH$ group of the choline cation. In the FT-IR spectrum of pure urea, vibrational bands at 3441 and 1567 cm^{-1} refer to the presence of N–H vibration. The characteristic C═O vibration can be found at 1662 cm^{-1}. The vibrational bands at 1457 cm^{-1} are assigned to C–N stretching of urea. During the formation of DES, the spectra of DES-CU is an overlap with those of both choline chloride and urea, and it illustrated that the structures of choline chloride and urea were not destroyed in DES-CU. Specifically, the small difference in wavenumbers compared to the signals of the N–H and C═O groups in urea and DES-CU indicates that hydrogen bonds were formed between choline chloride and urea.

In the FT-IR spectrum of pure ethylene glycol, vibrational bands at 3315 cm^{-1} refer to the presence of O–H vibration. The vibration bands at 2930 cm^{-1} are assigned to $–CH_2$ stretching of ethylene glycol (Fig. S3†). During the formation of DES, the spectrum of DES-CE overlaps with those of both choline chloride and ethylene glycol. It illustrated that the structures of choline chloride and ethylene glycol were not destroyed in DES-CE. Moreover, the absorption bands of DES-CE at 3440 cm^{-1} could be ascribed to the stretching vibration of the O–H functional group (Fig. S3†). There was a slight difference in the wavenumber compared to the signal of the O–H group in choline chloride as well as ethylene glycol, indicating that hydrogen bond formation was created between the two components of DES.

Thermal gravimetric analysis (TGA) from 50 to 750 °C showed that DES-CU started to decompose at around 150 °C (Fig. S4-A†). The major weight loss occurs in the temperature range from 150 to 350 °C. The decomposition temperature of both choline chloride and urea was found to be higher due to the formation of complexes of DES-CU. It was suggested that the DES obtained by the complexation of a quaternary ammonium salt and a hydrogen bond altered the properties of the choline chloride and urea.[46] DES exhibited a lower melting temperature than their individual components due to the weaker interaction between the choline cation and the correspondent hydrogen bond donors. Similarly, TGA showed that DES-CE started to decompose at around 150 °C. The major weight loss occurs between 150 and 300 °C. The decomposition of pure choline chloride and pure ethylene glycol was between 300 to 350 °C and 100 to 200 °C, respectively (Fig. S4-B†).

^{1}H NMR spectrum of DES-CU showed the resonances of choline chloride at 4.03–3.99 ppm (m, 2H) and 3.53–3.50 ppm (m, 2H), which were assigned to the $–CH_2–$ group of the choline cation. The signal at 3.23 ppm (s, 9H) was attributed to the $–CH_3$ resonance of the choline cation (Fig. S5†). The ^{1}H NMR spectrum of DES-CE indicated the resonances of choline chloride at 3.64–3.57 ppm (m, 2H), 3.31 ppm (m, 2H), and 3.74 ppm (s, 9H). The signal of ethylene glycol at 2.03 (9 s, 4H) showed $–CH_2–$, the resonance of the ethylene glycol (Fig. S6†). DES with high viscosities and several inter-and intra-dipolar interactions is the main reason for the broadening effect on the lineshape of the NMR spectrum. Additionally, the ^{1}H NMR spectrum shows that the structure of choline chloride and urea are not destroyed in DES-CU.

The glass transition temperature was determined using differential scanning calorimetry (DSC). The glass transition temperature depended strongly on the nature of the two components of DES. DSC spectrum of DES-CU under heating the deep eutectic mixture from −60 °C to 100 °C with a heating rate of 10 °C min^{-1} showed that there is an obvious exotherm with an onset temperature of −20 °C corresponding to the crystallization of glass (Fig. S7†). The process displayed one sharp melting endotherm with an onset temperature of 12 °C, which was consistent with the melting point. Obviously, DES-CU demonstrated two phase transitions from glass to crystal and crystal to melt during the DSC process. For DES-CE, the DSC spectrum showed that the glass transition temperature of the DES-CE mixture was from −34.62 °C (Fig. S8†).

B. IPCE and *J–V* characterization

Devices with different electrolytes showed similar IPCE spectra (Fig. 1). All devices had IPCE values of 50–60% at the spectrum band at around 540 nm, which was the characteristic IPCE peak of N719-sensitized cells. The IPCE spectra of CE and CU devices were a little bit lower than that of EMITCB. This might be due to the lower diffusion of I_3^- in CE and CU electrolytes than in EMITCB. The integrated current density values calculated from IPCE measurements are shown in Table 1. There was a small difference between the current density values from the *J–V* curves and the IPCE spectra. This could be due to the dissimilarity of light intensity between the two measurement systems.

The shape of *J–V* curves shows the photovoltaic performance of all devices, demonstrating that DES-CE and DES-CU could function well as solvents in DSC devices.[47] The forward and backward *J–V* curves were identical, indicating no hysteresis in the measurement (Fig. S9†). The J_{SC} of CE0.5 devices was 11.2 ± 0.3 mA cm^{-2}, comparable to 11.5 ± 0.3 mA cm^{-2} of EMITCB ones. EMITCB was considered a standard DSC ionic liquid solvent for its high J_{SC}, thanks to its low viscosity and high

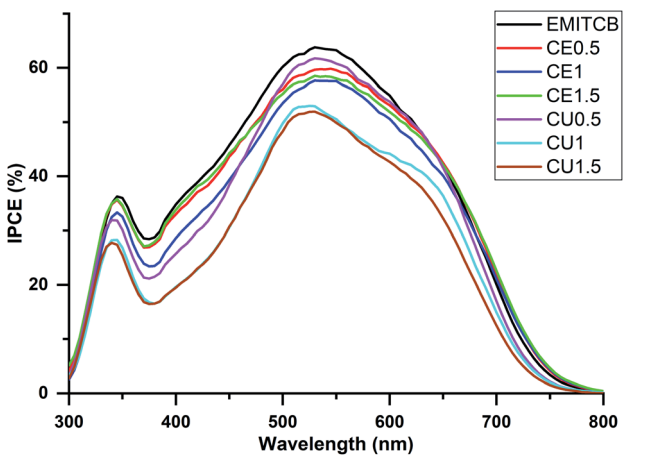

Fig. 1 IPCE spectra of DSC devices using EMITCB, CE, CU electrolytes.

Table 1 Cell parameters extracted from J–V curves of devices using EMITCB, CE0.5, CE1, CE1.5, CU0.5, CU1, and CU1.5 as electrolytes

	V_{OC} (mV)	J_{SC} (mA cm^{-2})	FF (%)	PCE (%)	J_{SC} (mA cm^{-2}) from IPCE
EMITCB	689 ± 1	11.5 ± 0.3	68 ± 2	5.4 ± 0.1	10.4 ± 0.1
CE0.5	658 ± 0	11.2 ± 0.3	69 ± 1	5.1 ± 0.2	9.9 ± 0.1
CE1	665 ± 9	10.0 ± 1.2	61 ± 3	4.0 ± 0.5	9.5 ± 0.1
CE1.5	648 ± 3	8.5 ± 1.9	67 ± 5	3.6 ± 0.6	9.9 ± 0.1
CU0.5	723 ± 2	10.3 ± 0.2	69 ± 2	5.1 ± 0.2	9.3 ± 0.2
CU1	745 ± 1	9.0 ± 0.3	64 ± 1	4.3 ± 0.2	7.6 ± 0.2
CU1.5	737 ± 3	5.7 ± 1.5	73 ± 8	3.0 ± 0.4	7.5 ± 0.1

conductivity, 18 cP (25 °C) and 15.1 mS cm^{-1} (20 °C),[48] respectively. In our study, DES-CE had viscosity 37 cP (25 °C)[47] and conductivity of 7.61 mS cm^{-1} (20 °C),[49] comparable to those of EMITCB. In contrast, the viscosity of DES-CU was 750 cP (25 °C), much higher than those of DES-CE and EMITCB. Furthermore, it had lower conductivity, 0.199 mS cm^{-1} (40 °C), than those of the other two solvents.[50] These underlied CU0.5's J_{SC} value of 10.3 ± 0.2 mA cm^{-2}, lower than that of CE0.5 (11.2 ± 0.3 mA cm^{-2}). However, the J_{SC} value of CU0.5 was still high compared to its disadvantageous nature, *e.g.*, its low viscosity. For the cells in the same electrolyte group, when increasing the amount of DES-CE by 3 times, J_{SC} dropped from 11.2 ± 0.3 mA cm^{-2} to 8.5 ± 1.9 mA cm^{-2} (Table 1). Moreover, it dropped nearly 50% of the initial value in the case of DES-CU.

The overall conversion efficiency of EMITCB was 5.4 ± 1%, the highest among the tested electrolytes. CE0.5 and CU0.5 achieved the same conversion efficiency, 5.1 ± 0.2%, which was a very competitive performance for any electrolyte at the same cost range as of these two. Even though the V_{OC} of CE0.5 devices was about 30 mV, lower than that of EMITCB, CE0.5 still achieved this impressive efficiency by maintaining a J_{SC} as high as that of the standard electrolyte. Although the initial J_{SC} of CU0.5 devices performed with J_{SC} was around 1 mA cm^{-2}, lower than that of CE0.5, it was maintained over a broader potential range (Fig. 2).

The fill factor value was strongly impacted by the series resistance,[51] but that was not the case for the observed results. Although the series resistance was around 20 Ω for all devices, the fill factor considerably varied between 60 to 70%.

Regarding the open-circuit potential (V_{OC}), the CU electrolyte group yielded the highest V_{OC} value, while the CE group had the V_{OC} value lower than EMITCB (Fig. 1). Considering CU1, CE1, and EMITCB electrolytes with an equivalent amount of solvents, the V_{OC} measured in CU1 was 745 ± 1 mV, significantly higher than EMITCB and CE1, 689 ± 1 mV and 665 ± 9 mV, respectively. Thus, DES-CU had a positive effect on improving the V_{OC}. We speculated that this effect might come from the restriction of charge leakage from the TiO_2–electrolyte interface, and proceeded to investigate with EIS analysis.

C. EIS of full cell in the dark

Under dark conditions with the applied bias voltage, dye-uncovered mesoporous TiO_2 electrode donates an electron to I_3^-, while the reduction of I_3^- to I^- occur at the Pt-FTO surface.[52] The charge transfer process at the Pt-FTO and electrolyte interface is described as a charge transfer resistance R_{CE} in parallel with a constant phase element CPE_{CE}. The charge transfer process at the TiO_2 electrode is a coupled parallel to R_{PE} and CPE_{PE}. The diffusion of I_3^- in the viscous electrolyte is modeled by a Warburg impedance element. R_S is the sum of all contact-resistant distributions (Fig. 3).

To reveal the influence of DES on the surface of TiO_2 and open circuit potential, we conducted EIS under various bias potentials. From this analysis, the CPE related to the charge

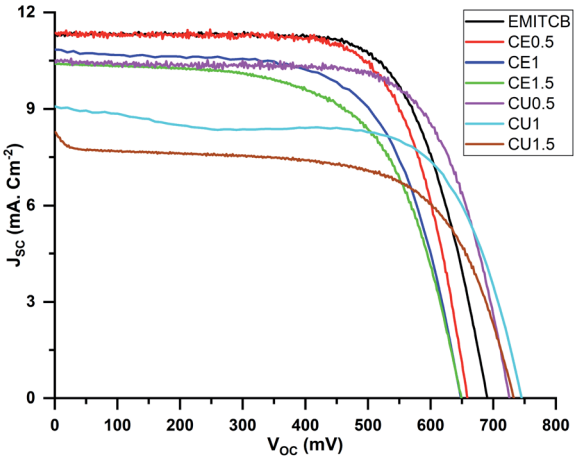

Fig. 2 Current–voltage characteristics of DSC devices using different electrolytes with various amounts of DES-CE, DES-CU compared to EMITCB. The light intensity was set at AM1.5, 100 mW cm^{-2}.

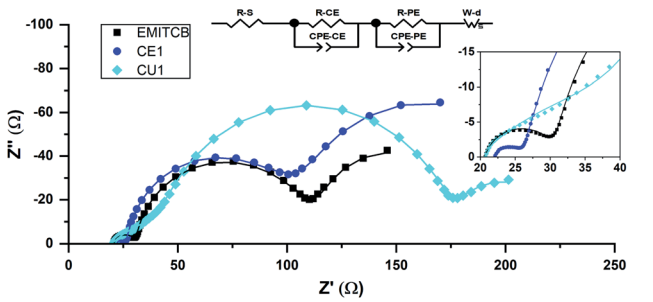

Fig. 3 Nyquist plot of DSC devices using EMITCB, CE1, CU1 electrolytes in dark condition under −0.7 V bias voltage. From left to right, the three arcs are related to the charge transfer process at the counter electrode–electrolyte interface, carrier transport at photoanode TiO_2|dye|electrolyte interfaces, and incomplete arc of electrolyte diffusion. The inset shows the enlarged first arcs. The dots are experimental points; lines are fitted experimental data with the equivalent circuit model attached in the figure.

accumulation on bare TiO_2 the surface was extracted and converted to the capacitance value by eqn (1)

$$C_{PE} = \frac{(CPE_{PE} \times R_{PE})^{CPE\text{-}P}}{R_{PE}} \quad (1)$$

where C_{PE} is the normalized TiO_2 interface charge capacitance; CPE_{PE} and CPE-P are the characteristic parameters describing the constant phase element; R_{PE} represents the charge transfer resistance at the TiO_2 interface.

C_{PE} is proportional exponentially to the bias voltage applied in the EIS measurement or the TiO_2 Fermi level as shown in eqn (2).[53]

$$C_{PE} = C_0 e^{\left[\frac{\alpha q}{k_B T} V_F\right]} \quad (2)$$

where α is the exponential electron trap distribution parameter; q is the electron charge; k_B is the Boltzmann constant; T is the temperature of the cell in kelvin; V_F is Fermi level of electrons in TiO_2; C_0 was calculated using eqn (3).[53]

$$C_0 = L(1-p)\alpha \frac{q^2 N_t}{k_B T} e^{\left[\frac{\alpha}{k_B T}(E_{redox} - E_c)\right]} \quad (3)$$

where L is the TiO_2 film thickness; p is the porosity of the film; N_t the total number of trap states below the conduction band; E_{redox} is the redox potential of I^-/I_3^-; E_c is the conduction band level of TiO_2 film.

The experimental interface capacitance points were well fitted by the exponential eqn (2) with the shortcut formula as $y = a \times e^{(-b \times x)}$ (Fig. 4A). Each electrolyte displayed different C curves of which the b values were proportional to the electron trap numbers. The application of a more negative potential on the anode increased the anode's electron density. Consequently, the density of oppositely charged ions at the interface (as shown in C values) and, with it, the probability of electron loss due to the ion exchange continued to surge.

As can be seen in Fig. 4A, the group of DES-CE had stronger capacitance curves banding upward corresponding to the more negative charge state of the TiO_2 electrode. Meanwhile, the DES-CU group curves lay under those of the EMITCB. It is worth noting that opposite trends were observed from the two groups of DES when different amounts of DES were used in the electrolytes. For the electrolytes of DES-CU, the density of oppositely charged ions at the interface was low (small b values), leading to lower electron loss probability and higher V_{OC}. The DES-CE electrolytes displayed the highest b values, meaning the highest electron trap distribution on the anode interface, with little variance. This was consistent with the lowest V_{OC} average with a small variance observed for these electrolytes. We suggested that these results could be explained due to the different molecular structures of the two DES.

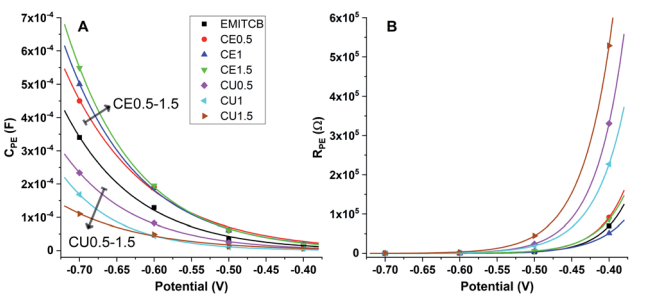

Fig. 4 (A) Interface capacitance of TiO_2 interface C_{PE}, and (B) charge transfer resistance of TiO_2 interface R_{PE} at various bias potentials under dark conditions. Experimental data (dot) were fitted (line) with R^2 = 0.99 and 1 for (A) and (B), respectively.

Ashish Pandey *et al.* reported that DES-CE with alcohol functional groups was more dipolar than DES-CU.[54] Although the polarity of these two solvents was not quantified, the results showed a correlation with conductivity, since polarity is an essential factor to determine the conductivity. Due to their higher polarity, components in DES-CE were more attracted by the negative charge at the TiO_2 interface, resulting in a higher possibility of charge release. For the same reason, DES-CE reached the highest charge density at the lowest potential among other solvents (Fig. 4A). Additionally, although an increasing percentage of DES-CE in the electrolytes diluted the I^-/I_3^- redox couple – the main electron carrier in DSC devices, the electrolyte could reach an even higher charge density at a lower applied voltage (Fig. 4A, arrow sign). However, the trend was observed oppositely when the amount of DES-CU was enhanced in the electrolyte.

The phenomenon observed with DES-CU was similar to the shielding effect, usually observed from conventional nitrogen heterocyclic additives such as *N*-methylbenzimidazole (NMB) or 4-*tert*-butylpyridine (4-TBP). NMB or 4-TBP could adsorb onto the TiO_2 surface causing the negative shift of the Fermi level of TiO_2, as well as preventing the triiodide penetration.[55–57] Notably, although NMB was present in all of the electrolytes in our study, its influence on V_{OC} was markedly different from each other. Thus, we speculated that DES-CU, which contains an amine functional group in urea, promoted the activity of NMB. Alternatively, DES-CU might act as an additive in DES electrolyte and help to improve V_{OC}. The effect of choline chloride on V_{OC} values as observed here could be eliminated as it was present both of DESs.

Using EMITCB's V_{OC} (689 mV) as the reference, we calculated the theoretical voltage of DSC devices *via* the fitted TiO_2 interface capacitance equations (Table 2). We assumed that the effect of the series resistance and the charge transfer resistance on TiO_2 conduction band shift were negligible compared to the influence of charge distribution and thus normalized the TiO_2 charge state of different electrolytes to the same condition. Consequently, the shielding efficiency of individual solvents EMITCB, CE, or CU could vary the activation energy of the charge transfer process at the TiO_2 interface and determine the required potential to reach the same charge density with the reference EMITCB.

Using the same concept as in the TiO_2 interface capacitance inspection, we plotted the TiO_2 interface charge transfer resistance as a function of the applied potential and fitted the experimental data by eqn (4) (Fig. 4B).[53]

Table 2 The potential of DES-CE and DES-CU devices was calculated *via* capacitance curve, with EMITCB's V_{OC} value as the reference

	EMITCB	CE0.5	CE1	CE1.5	CU0.5	CU1	CU1.5
Calculated potential (mV)	689	657	651	644	725	745	809
V_{OC} from *J–V* curves (mV)	689 ± 1	658 ± 0	665 ± 9	648 ± 3	723 ± 2	745 ± 1	737 ± 3

$$R_{PE} = R_0 e^{\left[\frac{\beta q}{k_B T} V_F\right]} \quad (4)$$

where β is the charge transfer coefficient for recombination of electrons and R_0 was calculated using eqn (5).[53]

$$R_0 = \frac{\sqrt{\pi \lambda k_B T}}{q^2 L \alpha k_r c_{I_3^-} N_s} e^{\left[\frac{\alpha}{k_B T}(E_c - E_{redox}) + \frac{\lambda}{4 k_B T}\right]} \quad (5)$$

where λ is the reorganization energy of the acceptor species; k_r is the rate constant of the recombination kinetics; $c_{I_3^-}$ is the concentration of I_3^-; N_s is the surface states involving recombination.

Our results showed that charge transfer resistance at the TiO_2 interface of DES-CU dramatically increased over the low potential area (Fig. 4B). As mentioned above, DES-CU was less polar than DES-CE and thus provided a good insulator environment under the internal electric field of the device. The lines of TiO_2 charge transfer resistance lay above the others showed that DES-CU devices displayed higher R_{PE}, indicating that these devices could resist the leakage current better than DES-CE and even EMITCB devices.

4. Conclusions

We prepared two choline chloride-based DESs with ethylene glycol and urea as room-temperature solvents for eco-friendly, inexpensive volatile solvent-free DSC electrolytes and under standard illumination achieved conversion efficiencies as high as 5.1 ± 0.2, comparable to that of the commercial ionic liquid EMITCB. DES-CE displayed higher J_{SC} than that of DES-CU thanks to its lower viscosity and much higher conductivity. In contrast, DES-CU, which contains an amine functional group, showed the shielding effect on TiO_2 interface. DES-CU not only played a role as a mediator solvent but also acted as an effective additive in the system that helps improve the V_{OC}. This noteworthy characteristic of DES-CU should be considered when designing other versatile DES-based electrolytes for eco-friendly DSCs with nonvolatile, non-flammable, low-cost, and scalable solvents. This type of DES-electrolyte is promising for large-scale production of DSC. Our work also demonstrated that the capacitance–potential curves from EIS could be used as a simple tool to estimate the theoretical V_{OC} values, with application potential in the high-throughput evaluation of electrolyte systems or additives on DSC devices.

Author contributions

De Nguyen: methodology, validation, investigation, writing – original draft. Tuan Van Huynh: methodology, investigation, formal analysis, writing – original draft. Vinh Son Nguyen: investigation, formal analysis. Phuong-Lien Doan Cao: investigation, formal analysis. Hai Truong Nguyen: formal analysis, writing – original draft, writing – review & editing. Tzu-Chien Wei: supervision, writing – review & editing. Phuong Hoang Tran: supervision, conceptualization, formal analysis, data curation, visualization, writing – review & editing. Phuong Tuyet Nguyen: funding acquisition, supervision, conceptualization, formal analysis, data curation, visualization, writing – review & editing.

Conflicts of interest

There are no conflicts to declare.

Acknowledgements

This research is funded by Vietnam National University HoChiMinh City (VNU-HCM) under grant number VL2020-18-04. The authors thank Dr Trinh-Don Nguyen for critically proofreading the manuscript.

References

1 B. O'Regan and M. Grätzel, *Nature*, 1991, **353**, 737–740.
2 A. Hagfeldt, G. Boschloo, L. Sun, L. Kloo and H. Pettersson, *Chem. Rev.*, 2010, **110**, 6595–6663.
3 J. Wu, Z. Lan, J. Lin, M. Huang, Y. Huang, L. Fan and G. Luo, *Chem. Rev.*, 2015, **115**, 2136–2173.
4 S. P. Mohanty and P. Bhargava, *Electrochim. Acta*, 2015, **168**, 111–115.
5 J. Preat, D. Jacquemin and E. A. Perpète, *Energy Environ. Sci.*, 2010, **3**, 891–904.
6 M. I. Asghar, K. Miettunen, J. Halme, P. Vahermaa, M. Toivola, K. Aitola and P. Lund, *Energy Environ. Sci.*, 2010, **3**, 418–426.
7 P. T. Nguyen, R. Degn, H. T. Nguyen and T. Lund, *Sol. Energy Mater. Sol. Cells*, 2009, **93**, 1939–1945.
8 P. T. Nguyen, A. R. Andersen, E. M. Skou and T. Lund, *Sol. Energy Mater. Sol. Cells*, 2010, **94**, 1582–1590.
9 P. T. Nguyen, B. X. T. Lam, A. R. Andersen, P. E. Hansen and T. Lund, *Eur. J. Inorg. Chem.*, 2011, **2011**, 2533–2539.
10 P. Wang, S. M. Zakeeruddin, J.-E. Moser and M. Grätzel, *J. Phys. Chem. B*, 2003, **107**, 13280–13285.
11 R. Kawano, H. Matsui, C. Matsuyama, A. Sato, M. A. B. H. Susan, N. Tanabe and M. Watanabe, *J. Photochem. Photobiol., A*, 2004, **164**, 87–92.
12 T. Lund, P. T. Nguyen, H. M. Tran, P. Pechy, S. M. Zakeeruddin and M. Grätzel, *Sol. Energy*, 2014, **110**, 96–104.

13 P. T. Nguyen, T. A. P. Phan, N. H. T. Ngo, T. V. Huynh and T. Lund, *Solid State Ionics*, 2018, **314**, 98–102.
14 P. T. Nguyen, N. P. D. Nguyen and L. T. Nguyen, *J. Phys. Chem. Solids*, 2018, **122**, 234–238.
15 W. Kubo, T. Kitamura, K. Hanabusa, Y. Wada and S. Yanagida, *Chem. Commun.*, 2002, 374–375, DOI: 10.1039/B110019J.
16 D. Zhao, Y. Liao and Z. Zhang, *Clean: Soil, Air, Water*, 2007, **35**, 42–48.
17 M. Bidikoudi, L. F. Zubeir and P. Falaras, *J. Mater. Chem. A*, 2014, **2**, 15326–15336.
18 C.-T. Li, C.-P. Lee, C.-T. Lee, S.-R. Li, S.-S. Sun and K.-C. Ho, *ChemSusChem*, 2015, **8**, 1244–1253.
19 H. H. Lin, J. D. Peng, V. Suryanarayanan, D. Velayutham and K. C. Ho, *J. Power Sources*, 2016, **311**, 167–174.
20 J.-D. Decoppet, S. B. Khan, M. S. A. Al-Ghamdi, B. G. Alhogbi, A. M. Asiri, S. M. Zakeeruddin and M. Grätzel, *Energy Technol.*, 2017, **5**, 321–326.
21 E. L. Smith, A. P. Abbott and K. S. Ryder, *Chem. Rev.*, 2014, **114**, 11060–11082.
22 A. P. Abbott, J. C. Barron, K. S. Ryder and D. Wilson, *Chem.–Eur. J.*, 2007, **13**, 6495–6501.
23 A. P. Abbott, D. Boothby, G. Capper, D. L. Davies and R. K. Rasheed, *J. Am. Chem. Soc.*, 2004, **126**, 9142–9147.
24 A. P. Abbott, G. Capper, D. L. Davies, R. K. Rasheed and V. Tambyrajah, *Chem. Commun.*, 2003, 70–71.
25 W. Guo, Y. Hou, S. Ren, S. Tian and W. Wu, *J. Chem. Eng. Data*, 2013, **58**, 866–872.
26 E. L. Smith, A. P. Abbott and K. S. Ryder, *Chem. Rev.*, 2014, **114**, 11060–11082.
27 L. I. N. Tomé, V. Baião, W. da Silva and C. M. A. Brett, *Appl. Mater. Today*, 2018, **10**, 30–50.
28 B.-Y. Zhao, P. Xu, F.-X. Yang, H. Wu, M.-H. Zong and W.-Y. Lou, *ACS Sustainable Chem. Eng.*, 2015, **3**, 2746–2755.
29 S. Khandelwal, Y. K. Tailor and M. Kumar, *J. Mol. Liq.*, 2016, **215**, 345–386.
30 B. L. Gadilohar and G. S. Shankarling, *J. Mol. Liq.*, 2017, **227**, 234–261.
31 P. Vitale, V. M. Abbinante, F. M. Perna, A. Salomone, C. Cardellicchio and V. Capriati, *Adv. Synth. Catal.*, 2017, **359**, 1049–1057.
32 K. O. Wikene, H. V. Rukke, E. Bruzell and H. H. Tonnesen, *J. Photochem. Photobiol., B*, 2017, **171**, 27–33.
33 O. S. Hammond, K. J. Edler, D. T. Bowron and L. Torrente-Murciano, *Nat. Commun.*, 2017, **8**, 14150–14157.
34 C. Vidal, L. Merz and J. García-Álvarez, *Green Chem.*, 2015, **17**, 3870–3878.
35 W.-H. Zhang, M.-N. Chen, Y. Hao, X. Jiang, X.-L. Zhou and Z.-H. Zhang, *J. Mol. Liq.*, 2019, **278**, 124–129.
36 M. J. Rodríguez-Álvarez, J. García-Álvarez, M. Uzelac, M. Fairley, C. T. O'Hara and E. Hevia, *Chem.–Eur. J.*, 2018, **24**, 1720–1725.
37 J. Chen, M. Liu, Q. Wang, H. Du and L. J. M. Zhang, *Molecules*, 2016, **21**, 1383.
38 A. H. Panhwar, M. Tuzen and T. G. Kazi, *Talanta*, 2018, **178**, 588–593.
39 R. A. Zounr, M. Tuzen, N. Deligonul and M. Y. Khuhawar, *Food Chem.*, 2018, **253**, 277–283.
40 D. Carriazo, M. C. Serrano, M. C. Gutiérrez, M. L. Ferrer and F. del Monte, *Chem. Soc. Rev.*, 2012, **41**, 4996–5014.
41 H.-R. Jhong, D. S.-H. Wong, C.-C. Wan, Y.-Y. Wang and T.-C. Wei, *Electrochem. Commun.*, 2009, **11**, 209–211.
42 C. L. Boldrini, N. Manfredi, F. M. Perna, V. Trifiletti, V. Capriati and A. Abbotto, *Energy Technol.*, 2017, **5**, 345–353.
43 P. T. Nguyen, T.-D. T. Nguyen, V. S. Nguyen, D. T.-X. Dang, H. M. Le, T.-C. Wei and P. H. Tran, *J. Mol. Liq.*, 2019, **277**, 157–162.
44 G. García, S. Aparicio, R. Ullah and M. Atilhan, *Energy Fuels*, 2015, **29**, 2616–2644.
45 J.-L. Lan, C.-C. Wan, T. C. Wei, W.-C. Hsu, C. Peng, Y.-H. Chang and C.-M. Chen, *Int. J. Electrochem. Sci.*, 2011, **6**, 1230–1236.
46 O. S. Hammond, D. T. Bowron and K. J. Edler, *Green Chem.*, 2016, **18**, 2736–2744.
47 C. D'Agostino, R. C. Harris, A. P. Abbott, L. F. Gladden and M. D. Mantle, *Phys. Chem. Chem. Phys.*, 2011, **13**, 21383–21391.
48 S. Seki, N. Serizawa, K. Hayamizu, S. Tsuzuki, Y. Umebayashi, K. Takei and H. Miyashiro, *J. Electrochem. Soc.*, 2012, **159**, A967–A971.
49 A. P. Abbott, R. C. Harris and K. S. Ryder, *J. Phys. Chem. B*, 2007, **111**, 4910–4913.
50 A. P. Abbott, G. Capper and S. Gray, *ChemPhysChem*, 2006, **7**, 803–806.
51 Q. Wang, S. Ito, M. Grätzel, F. Fabregat-Santiago, I. Mora-Seró, J. Bisquert, T. Bessho and H. Imai, *J. Phys. Chem. B*, 2006, **110**, 25210–25221.
52 Q. Wang, J.-E. Moser and M. Grätzel, *J. Phys. Chem. B*, 2005, **109**, 14945–14953.
53 S. R. Raga, E. M. Barea and F. Fabregat-Santiago, *J. Phys. Chem. Lett.*, 2012, **3**, 1629–1634.
54 A. Pandey, R. Rai, M. Pal and S. Pandey, *Phys. Chem. Chem. Phys.*, 2014, **16**, 1559–1568.
55 T. Stergiopoulos, E. Rozi, C.-S. Karagianni and P. Falaras, *Nanoscale Res. Lett.*, 2011, **6**, 307.
56 H. Kusama and H. Arakawa, *J. Photochem. Photobiol., A*, 2004, **162**, 441–448.
57 T. A. P. Phan, N. P. Nguyen, L. T. Nguyen, P. H. Nguyen, T. K. Le, T. V. Huynh, T. Lund, D.-H. Tsai, T.-C. Wei and P. T. Nguyen, *Appl. Surf. Sci.*, 2020, **509**, 144878.